Comparative study of lithium-ion battery open-circuit-voltage online estimation methods

Jianwen Meng, Moussa Boukhnifer, Demba Diallo

IET Electrical Systems in Transportation

Research Article

IET Journals
The Institution of Engineering and Technology

Comparative study of lithium-ion battery open-circuit-voltage online estimation methods

ISSN 2042-9738
Received on 21st January 2019
Revised 24th September 2019
Accepted on 16th October 2019
E-First on 18th December 2019
doi: 10.1049/iet-est.2019.0026
www.ietdl.org

Jianwen Meng[1,2] ✉, *Moussa Boukhnifer*[3], *Demba Diallo*[2,4]

[1]*ESTACA, Ecole d'ingénieurs, 12 avenue Paul Delouvrier, 78066 Saint-Quentin-en-Yvelines, France*
[2]*GeePs | Group of Electrical Engineering – Paris, CNRS, CentraleSupélec, Univ. Paris-Sud, Université Paris-Saclay, Sorbonne Université, 3 & 11 rue Joliot-Curie, Plateau de Moulon 91192 Gif-sur-Yvette CEDEX, France*
[3]*Université de Lorraine, LCOMS EA 7306, Metz, 57000, France*
[4]*Shanghai Maritime University, Department of Electrical Automation, 201306 Shanghai, People's Republic of China*
✉ *E-mail: Jianwen.MENG@estaca.fr*

Abstract: As an important property and distinct characteristic of different lithium-ion batteries, open-circuit-voltage (OCV) online estimation can provide useful information for battery monitoring and fault diagnosis. However, studies dedicated to battery OCV estimation are not as much as the research efforts on state-of-charge determination and parameter identification such as capacity and resistance. Hence, a general discussion for selecting the battery OCV estimation algorithm is proposed in this study. To this end, modelling process of extended state-space model and autoregressive exogenous model is presented in detail. Four estimation algorithms, namely, Luenberger observer, Kalman filter, recursive least-square with forgetting factor and recursive least-square with variable forgetting factor are selected and compared in terms of estimation accuracy, computational cost, parameter tuning and robustness to parameter variations. Based on real battery cell parameters and environmental conditions, simulation results have shown that even if they are less robust to model uncertainty, observer-based methods exhibit better estimation performances than regression-based ones.

1 Introduction

Lithium-ion batteries (LIBs), which can be used as the principal energy source in battery electric vehicles (BEVs) or the auxiliary energy module in hybrid electric vehicles (HEVs), have been massively used for onboard energy storage systems due to their relatively high power and energy density, eco-friendly characteristic and promising potential for cost reduction [1]. Various research works around LIBs have been carried out on a large scale, while from the perspective of control, LIB online monitoring, including battery state and parameter estimation, is fundamental and necessary for the follow-up works such as battery fault detection and battery health prognosis.

Normally, the aforementioned real-time battery monitoring mission is model-based, which is suitable for the processing capability of current embedded chips of the vehicle battery management system (BMS) [2]. Compared with the electrochemical models, equivalent circuit models (ECMs) are more attractive because of their simplicity and reliability. The ECM composed of an open-circuit-voltage (OCV) source connected in series with a resistor and one or more RC network(s) is widely used to reproduce the battery's electrical behaviour, and to further accomplish the objective of state and parameter estimation [3–6].

The OCV, an important term that represents the distinct characteristic of different LIBs, can be regarded as one of the parameters to be estimated in battery ECM and whose story should be started from the battery state-of-charge (SOC) estimation.

As a replacement for the fuel gauge used in traditional vehicles, battery SOC, which is commonly defined as the percentage of the maximum possible charge that is present inside a rechargeable battery, is a key indicator that should be determined during the operation [7]. Because it will be used to design the battery EMS, and can further avoid the emergence of over-charge and over-discharge problems in LIBs, which could be the root of violent thermal runaways [8]. However, its indirectly measurable characteristic makes the relevant SOC estimation methods appear.

The traditional ampere-hour (AH) counting method is a classical real-time SOC estimation technique, where the required SOC can be determined by integrating the flowing current with the known battery capacity and an accurate initial SOC value [1]. However, the open-loop mechanism will cause the AH counting method to have accumulated estimation errors over a long period of time, because it is inevitably affected by the current noise, the uncertain initial SOC value as well as the rated current battery capacity, which will change with various factors such as temperature, aging degree and so on [9].

Therefore, in order to overcome this drawback, the AH counting method is usually combined with an OCV-based SOC estimation method, whose working principle is a voltage-look-up process that based on the simple one-to-one relationship between battery OCV and SOC [10]. The measured battery OCV can infer the corresponding SOC, which can be used as a periodic calibration for the AH counting method [11]. Hence, the combination of these two methods constitutes an efficient approach for determining the battery SOC in the application of BEVs and HEVs [1].

However, an accurate measurement of the OCV requires LIBs to stay in open-circuit conditions for a sufficient long period of time, which usually takes several hours [12]. In fact, this is because the so-called OCV relaxation process after the current interruption. To be short, when the battery is charging or discharging, its internal states (micro-level) will be disturbed by the external excitation; while after the external current is interrupted, it will consequently take time for the battery to rebuild a new equilibrium state, which is fixed as electromotive force (EMF) [13, 14]. In other words, the OCV that usually appears in the literature is approximately the EMF in the equilibrium state after the OCV relaxation process [14].

Furthermore, the aforementioned relaxation process strongly depends on the short time previous usage history, including the current value and the current direction, and the latter can cause the well-known OCV hysteresis phenomenon. Specifically, the OCV relaxation process is under the EMF if the battery is previously discharged; on the contrary, it is above the EMF if the battery is previously charged [13]. However, even though there exist the

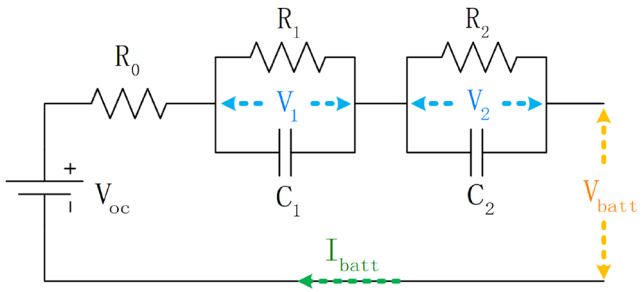

Fig. 1 *Battery ECM with double-RC network*

relevant hysteresis models for the OCV, the battery will never operate along these two hysteresis curves in reality due to the more complicated hysteresis 'eye' phenomenon (also called 'minor loop') [15, 16]. Moreover, other factors such as temperature, initial SOC and battery technology (e.g. the LIB with $LiFePO_4$ cathode has serious hysteresis phenomenon) will also affect the OCV relaxation process [13, 15].

Obviously, previously mentioned complicated indescribable physical phenomenon would largely affect OCV measurement results; besides, the long waiting time is an obstacle for developing OCV-based SOC estimation method. Fortunately, based on battery ECM, real-time battery SOC determination through OCV-SOC look-up table becomes possible when various adaptive estimation methods of battery OCV are introduced. In fact, not only do they greatly shorten the OCV measurement time, but also make the OCV-based SOC estimation method become an independent SOC online determination method, which belongs to the model-based SOC estimation method that only uses measurable battery signals such as voltage, current and temperature [1].

Broadly speaking, online OCV estimation techniques can be divided into two families, namely, observer-based and regression-based methods. For instance, in [5], extended Kalman filter (EKF) is employed to execute online parameter identification as well as OCV estimation; in [17], H_∞ filter is applied to obtain the OCV curve within 2 s instead of using the traditional OCV tests such as incremental OCV or low-current OCV test which usually takes 3–5 days. On the other hand, the classical recursive least-squares (RLS) algorithm and its numerous variations can also realise OCV estimation. For example, the U-D factorised-based RLS is applied to estimate the OCV, which is further used to infer the battery SOC in [18]. In [19], multiple adaptive forgetting factors RLS, which can cope with the different varying rates of different parameters, is proposed in order to distribute a forgetting factor to each parameter that needs to be estimated.

However, in the literature, most of the research efforts are focused on model-based SOC estimation and on-line parameter identification such as capacity and resistance. Therefore, we are hereafter interested in developing a battery OCV estimation algorithm. The main contributions of this paper are as follows:

(i) Characteristics and main properties of battery OCV are reviewed in the introduction.
(ii) Modelling process of extended battery ECM and autoregressive exogenous (ARX) model is presented.
(iii) The principle of the estimation algorithms is summarised into one diagram, which can concisely illustrate the observer-based and regression-based estimation algorithms. Based on this comparative study, the advantages and disadvantages of observer-based and regression-based estimation algorithms for estimating battery OCV are pointed out.

The remainder of our work is organised as follows: the battery model for observer-based and regression-based OCV estimation methods is detailed in Section 2. In Section 3, OCV estimation algorithms, namely, Luenberger observer (LO), Kalman filter (KF), RLS with forgetting factor (FF-RLS) and RLS with variable forgetting factor (VFF-RLS), will be introduced; then, simulation studies including parameter tuning and comparison of estimation methods will be presented in Sections 4 and 5. A conclusion will end this paper.

2 Battery modeling

A second-order battery ECM, as shown in Fig. 1, is retained for OCV estimation in this paper. The model is described as follows:

(i) The resistor R_0 stands for the ohmic resistance, which includes resistance of contacts, electrodes as well as electrolytes [3].
(ii) The double pair RC characterises the charge transfer effect, the diffusion effect and double-layer behaviour inside LIBs. It simulates the battery transient response. Besides, the double RC-network is a good trade-off between the model error and the model complexity compared with single-RC and triple-RC structures [20].
(iii) The voltage source V_{oc} represents the OCV, which mainly depends on the battery SOC. Its average value is usually a monotonically increasing function of the SOC [3].

According to Kirchhoff's law, the discretised ECM state-model is given by (1). It is obtained with the zero-order hold approximation under the assumption that the current I_{batt} is constant between two adjacent sampling points [20]

$$\begin{cases} \begin{bmatrix} V_1(k) \\ V_2(k) \end{bmatrix} = \boldsymbol{A} \begin{bmatrix} V_1(k-1) \\ V_2(k-1) \end{bmatrix} + \boldsymbol{B} I_{batt}(k-1) \\ V_{batt}(k) - V_{oc} = \boldsymbol{C} \begin{bmatrix} V_1(k) \\ V_2(k) \end{bmatrix} + D I_{batt}(k) \end{cases} \tag{1}$$

where

$$\boldsymbol{A} = \begin{bmatrix} e^{-T/R_1C_1} & 0 \\ 0 & e^{-T/R_2C_2} \end{bmatrix} = \begin{bmatrix} a_1 & 0 \\ 0 & a_2 \end{bmatrix}$$

$$\boldsymbol{B} = \begin{bmatrix} R_1(1-e^{-T/R_1C_1}) \\ R_2(1-e^{-T/R_2C_2}) \end{bmatrix} = \begin{bmatrix} b_1 \\ b_2 \end{bmatrix}$$

$$\boldsymbol{C} = [-1, -1]$$

$$D = -R_0$$

and V_1 and V_2 are the voltages across capacitors C_1 and C_2, respectively; I_{batt} is the input current, according to its reference direction in Fig. 1, '+' means discharging process, while '–' means charging process; V_{batt} is the output voltage of the battery; T, the sampling time period for the discrete-time system, is set to 1 s in this work.

Furthermore, in order to estimate the V_{oc}, it is assumed that $dV_{oc}/dt \simeq 0$. The reasonable explanation can be given as follows [21]: firstly, as it is well known, all the parameters of battery ECM, including the OCV, will change with the temperature *Temp*, SOC and the usage history H; consequently, the relationship $V_{oc} = p(Temp, soc, H)$ can be analysed here, where $p(\cdot)$ is a nonlinear function and *soc* is the operator of SOC; then, the differential of $p(\cdot)$ with respect to time t is shown in the following equation:

$$\frac{dV_{oc}}{dt} = \frac{\partial p}{\partial Temp} \cdot \frac{\partial Temp}{\partial t} + \frac{\partial p}{\partial soc} \cdot \frac{\partial soc}{\partial t} + \frac{\partial p}{\partial H} \cdot \frac{\partial H}{\partial t} \tag{2}$$

Equation (2) equals zero with the following assumptions [21]: (a) due to the battery cooling system, the LIBs' temperature changes slowly to avoid heavy thermal stress, then $\partial Temp/\partial t \simeq 0$ becomes true consequently; (b) a general example of city-EV given in [21] shows that $\partial soc/\partial t \simeq -0.00028$, which means only a small amount of the battery energy is consumed, hence $\partial soc/\partial t \simeq 0$; (c) $\partial H/\partial t \simeq 0$ definitely holds since the long usage history of LIB is considered. As a result, V_{oc} can be reasonably regarded as almost constant to build the models for the observer-based and regression-based estimation methods.

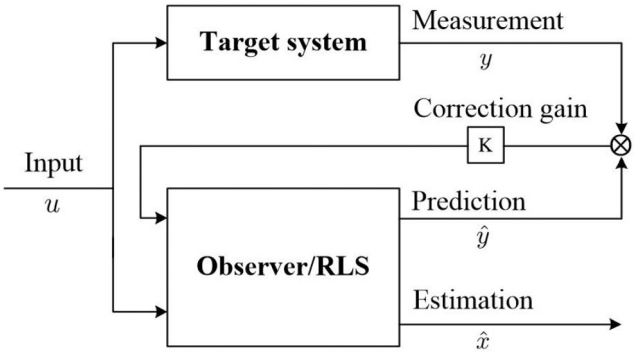

Fig. 2 *Schematic diagram of the 'prediction–correction' principle*

2.1 Extended battery ECM

As a symbol of modern control theory, state-space representation can not only be the basis for advanced observers, but also provides the convenience for estimating the slowly varying unmeasurable parameters. This means that the extended model is obtained by adding the unknown parameters as additional state variables with the aforementioned zero-time derivatives [22]. Notice that there is no distinction between these parameters and the other state variables. However, the structural simplicity of this solution is achieved at the price of introducing the hyperspace, which is usually a quantity of very high dimensions [22].

As for the battery OCV estimation in this work, the extended battery ECM based on (1) is built as follows:

$$\begin{cases} \begin{bmatrix} V_1(k) \\ V_2(k) \\ V_{\text{oc}}(k) \end{bmatrix} = \boldsymbol{F} \begin{bmatrix} V_1(k-1) \\ V_2(k-1) \\ V_{\text{oc}}(k-1) \end{bmatrix} + \boldsymbol{G} I_{\text{batt}}(k-1) \\ V_{\text{batt}}(k) = \boldsymbol{H} \begin{bmatrix} V_1(k) \\ V_2(k) \\ V_{\text{oc}}(k) \end{bmatrix} + J I_{\text{batt}}(k) \end{cases} \tag{3}$$

where

$$\boldsymbol{F} = \begin{bmatrix} e^{-T/R_1C_1} & 0 & 0 \\ 0 & e^{-T/R_2C_2} & 0 \\ 0 & 0 & 1 \end{bmatrix}, \quad \boldsymbol{G} = \begin{bmatrix} R_1(1-e^{-T/R_1C_1}) \\ R_2(1-e^{-T/R_2C_2}) \\ 0 \end{bmatrix}$$
$$\boldsymbol{H} = [-1, -1, 1], \quad J = -R_0$$

Obviously, the extended battery model (3) is linear, where the battery OCV could be estimated along with the other two battery states during the operation. Note that there is no assumption on the linearity of the OCV-SOC curve during the battery modelling process. The linear model is obtained with the help of the general expression $\mathrm{d}V_{\text{oc}}/\mathrm{d}t \simeq 0$.

2.2 ARX model

For the purpose of applying the regression-based method, z-transform pairs for the discrete-time system (1) between time-domain and frequency-domain is used to deduce the required ARX model for estimating the battery OCV [18, 19, 23]

$$\begin{aligned} \frac{Y(z)}{U(z)} &= [\boldsymbol{C}(z\boldsymbol{I} - \boldsymbol{A})^{-1}\boldsymbol{B} + D] \\ \frac{V_{\text{batt}}(z) - V_{\text{oc}}}{I_{\text{batt}}(z)} &= \left[\frac{b_1(a_2 - z) + b_2(a_1 - z)}{(z - a_1)(z - a_2)} - R_0\right] \end{aligned} \tag{4}$$

where $\boldsymbol{A}$, $\boldsymbol{B}$, $\boldsymbol{C}$ and D are the corresponding matrixes and scalar of (1); $\boldsymbol{I}$ is a unit matrix with the corresponding dimension; $Y(z)$ and $U(z)$ are the output and input of (1) in the z-domain corresponding to $V_{\text{batt}}(k) - V_{\text{oc}}$ and $I_{\text{batt}}(k)$, respectively, in the time-domain; z is the z-transform operator. Note that V_{oc} is regarded as a constant during the transformation process, which has been explained previously.

Applying the inverse z-transform ($x[n-k] \Leftrightarrow z^{-k}x(z)$) for (4), the following differential equation can be obtained after simplification and recombination:

$$\begin{aligned} V_{\text{batt}}(k) &= (a_1 + a_2)V_{\text{batt}}(k-1) \\ &\cdots - a_1a_2V_{\text{batt}}(k-2) - R_0I_{\text{batt}}(k) \\ &\cdots + (R_0a_1 + R_0a_2 - b_1 - b_2)I_{\text{batt}}(k-1) \\ &\cdots + (b_1a_2 + b_2a_1 - R_0a_1a_2)I_{\text{batt}}(k-2) \\ &\cdots + (1 - a_1 - a_2 + a_1a_2)V_{\text{oc}} \end{aligned} \tag{5}$$

Consequently, the ARX model of the battery can be obtained by rewriting (5) in the following form:

$$V_{\text{batt}}(k) = \boldsymbol{\varphi}'(k)\boldsymbol{\theta} \tag{6}$$

with
$\boldsymbol{\varphi} = [V_{\text{batt}}(k-1), V_{\text{batt}}(k-2), I_{\text{batt}}(k), I_{\text{batt}}(k-1), I_{\text{batt}}(k-2), 1]'$;
$\boldsymbol{\theta} = [\theta_1, \theta_2, \theta_3, \theta_4, \theta_5, \theta_6]'$, where

$$\begin{aligned} \theta_1 &= a_1 + a_2, \\ \theta_2 &= -a_1a_2, \\ \theta_3 &= -R_0, \\ \theta_4 &= R_0a_1 + R_0a_2 - b_1 - b_2, \\ \theta_5 &= b_1a_2 + b_2a_1 - R_0a_1a_2, \\ \theta_6 &= (1 - a_1 - a_2 + a_1a_2)V_{\text{oc}}, \end{aligned} \tag{7}$$

and the battery OCV can be deduced as

$$V_{\text{oc}} = \frac{\theta_6}{(1 - a_1 - a_2 + a_1a_2)} = \frac{\theta_6}{(1 - \theta_1 - \theta_2)} \tag{8}$$

In fact, (6) is a simple linear mathematical model where $V_{\text{batt}}(k)$ is the measurable signal, $\boldsymbol{\theta}$ is the parameter vector to be determined, the known vector $\boldsymbol{\varphi}(k)$ is called regression variables or regressors [22].

3 OCV estimation algorithm

For observer-based or regression-based estimation algorithms, although there exist different explanations such as Bayesian inference [24], geometric interpretation [22], etc., both of them can be illustrated intuitively by the following 'prediction–correction' principle [22, 25, 26].

In Fig. 2, the estimation process of a state variable is given as an example, where the core is the sustained error correction mechanism that is composed of a correction gain K multiplied by the error between the measurement and prediction, namely, y and $\hat{y}$. Then, broadly speaking, estimation algorithms differ in how to calculate the gain K in order to guarantee the convergence of the estimated state $\hat{x}$ only with the known information such as system input u and output y.

3.1 Luenberger observer

LO, as one of the most implemented real-time state observers for the linear system, is relevant to use in this case due to the linear characteristic of the extended battery model (3). Because of the off-line determination of the observer gain, there is less calculation stress for the vehicle BMS [4].

The estimated vector $\hat{\boldsymbol{x}}$ by the LO at the sample k is given by [4]

$$\hat{\boldsymbol{x}}_k = \boldsymbol{f}(\hat{\boldsymbol{x}}_{k-1}, u_{k-1}) + \boldsymbol{K}(y_{k-1} - \hat{y}_{k-1}) \tag{9}$$

where $\boldsymbol{f}(\cdot)$ is the linear function of the target system and $\boldsymbol{K}$ is the observer gain, as shown in Fig. 2. The gain is computed by the

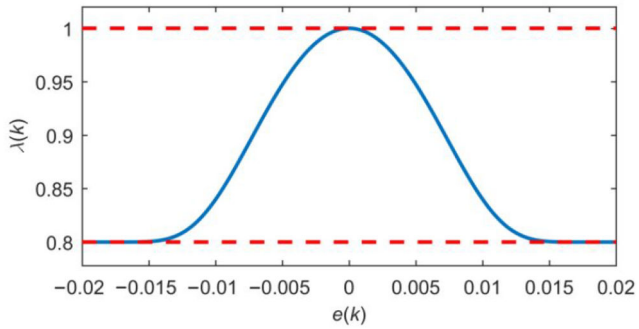

Fig. 3 *Mechanism of the variable forgetting factor λ(k) [28]*

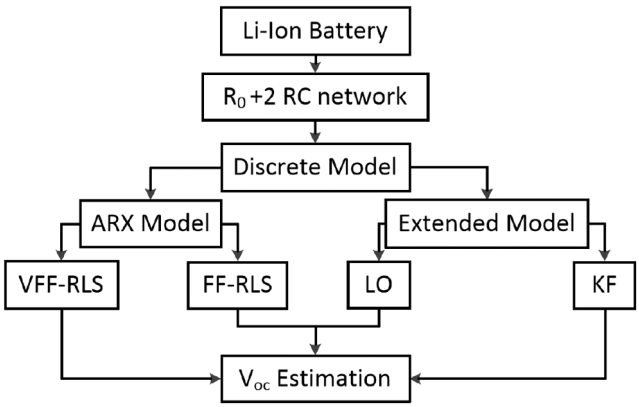

Fig. 4 *Flowchart of this comparative study*

classical pole placement strategy to achieve the desired performance [23].

3.2 Kalman filter

KF is a classical observer that has been recognised as an optimal state estimation technique for tracking the state of an uncertain dynamic system [27]; one of the characteristics of KF is that the Gaussian independent white noises are considered both in the state space and the output equations.

As shown in (10), and adapted the general form of linear system according to the model in (3) is given in order to present the classical recursive algorithm of KF

$$\begin{aligned} \boldsymbol{x}_k &= \boldsymbol{F}\boldsymbol{x}_{k-1} + \boldsymbol{G}u_{k-1} + \boldsymbol{w}_{k-1} \\ y_k &= \boldsymbol{H}\boldsymbol{x}_k + \mathrm{J}u_k + v_k \end{aligned} \tag{10}$$

where $\boldsymbol{w}_k$ is a vector that represents the zero-mean white process noise with covariance matrix $\boldsymbol{Q}$; v_k is the zero-mean white measurement scalar noise with covariance R.

Therefore, the linear Kalman filtering process is shown as follows [24]:

1. Prediction:
$$\hat{\boldsymbol{x}}_k^- = \boldsymbol{F}\hat{\boldsymbol{x}}_{k-1} + \boldsymbol{G}u_{k-1}$$
$$\boldsymbol{P}_k^- = \boldsymbol{F}\boldsymbol{P}_{k-1}\boldsymbol{F}' + \boldsymbol{Q}$$
2. Gain computation:
$$\boldsymbol{K}_k = \boldsymbol{P}_k^-\boldsymbol{H}'[\boldsymbol{H}\boldsymbol{P}_k^-\boldsymbol{H}' + R]^{-1}$$
3. Update:
$$\hat{\boldsymbol{x}}_k = \hat{\boldsymbol{x}}_k^- + \boldsymbol{K}_k[y_k - (\boldsymbol{H}\hat{\boldsymbol{x}}_k^- + Ju_k)]$$
$$\boldsymbol{P}_k = (\boldsymbol{I} - \boldsymbol{K}_k\boldsymbol{H})\boldsymbol{P}_k^-$$

where $\hat{\boldsymbol{x}}_k^-$ and $\boldsymbol{P}_k^-$ are, respectively, the priori state and error covariance estimates; $\boldsymbol{K}_k$ is the feedback gain for the KF, which is recursively calculated at each time step forcing the estimator to converge faster [4]; $\boldsymbol{P}_k$ is the estimation error covariance matrix.

3.3 RLS with fixed forgetting factor

The classical parameter identification technique by the least-squares method, whose principle has been formulated at the end of the eighteenth century, can be applied to a large variety of problems [22]. With sequential pairs of observations and regressors $\{(y(i), \varphi(i), i = 1, 2, \ldots, k)\}$, and considering the slowly time-varying parameters in the system, the estimated parameter vector $\hat{\boldsymbol{\theta}}(k)$ by the traditional FF-RLS is given directly [22]

$$\begin{aligned} \hat{\boldsymbol{\theta}}(k) &= \hat{\boldsymbol{\theta}}(k-1) + \boldsymbol{K}(k)[y(k) - \boldsymbol{\varphi}'(k)\hat{\boldsymbol{\theta}}(k-1)] \\ \boldsymbol{K}(k) &= \frac{\boldsymbol{P}(k-1)\boldsymbol{\varphi}(k)}{\lambda + \boldsymbol{\varphi}'(k)\boldsymbol{P}(k-1)\boldsymbol{\varphi}(k)} \\ \boldsymbol{P}(k) &= \frac{\boldsymbol{P}(k-1) - \boldsymbol{K}(k)\boldsymbol{\varphi}'(k)\boldsymbol{P}(k-1)}{\lambda}, \quad (\lambda \neq 0) \end{aligned} \tag{11}$$

where $\lambda \in \{\lambda_{\min}, 1\}$ is called the forgetting factor that can cope with the system's slow parametric varying characteristic. In other words, it implies that a time-varying weighting of data is introduced: the most recent data is given a unit weight, but data that is n time units old is weighted by λ^n [22]. In fact, a smaller value of λ induces a higher impact of the latest data, which means FF-RLS can track the changes of parameters quickly, but the stability of the algorithm is reduced. On the contrary, a higher value of λ can increase the stability of the algorithm, but the ability to track the time-varying parameters is weak [28].

3.4 RLS with variable forgetting factor

It has been pointed out that the performance of FF-RLS relies significantly on the forgetting factor λ in terms of convergence and stability [19]. However, the requirements for the forgetting factor depend on the application. There are, therefore various adaptive strategies [28]. The selected variable forgetting factor strategy from [28] is shown in (12), which combined with the traditional FF-RLS constitutes the VFF-RLS

$$\begin{aligned} \lambda(k) &= \lambda_{\min} + (1 - \lambda_{\min})^{\alpha(k)} \\ \alpha(k) &= 2^{\rho e^2(k)} \\ e(k) &= y(k) - \boldsymbol{\varphi}'(k)\hat{\boldsymbol{\theta}}(k) \end{aligned} \tag{12}$$

where $\lambda_{\min}$ and ρ are two fixed parameters [28].

An example from [28], as illustrated in Fig. 3, can clearly explain this varying mechanism. The forgetting factor will change according to the error $e(k)$ between the measured and estimated output, which means when $e(k)$ approaches 0, $\alpha(k)$ and $\lambda(k)$ tend to 1; when $e(k)$ tends to infinity, $\alpha(k)$ also tends to infinity and $\lambda(k)$ tends to $\lambda_{\min}$ [28].

In addition, the curve's shape in Fig. 3 is affected by the selected fixed parameters $\lambda_{\min}$ and ρ; the higher ρ is, the more sensitive $\lambda(k)$ is to $e(k)$ [28]. Therefore, in [28], the author has set these two parameters by minimising the following criterion:

$$J_o = \sum_{k=1}^{L} [y(k) - \varphi'(k)\hat{\theta}]^2 \tag{13}$$

where L is the number of observations [28].

A flowchart of this comparative study is displayed in Fig. 4.

4 Simulation results

The used LIB parameters in the simulations are derived from [29], including a seventh-order polynomial OCV model which is a monotonically increasing function of SOC (see (14)) . It is worth noting that (14) is the average OCV value of the charge and discharge process. Therefore, the hysteresis effect is ignored here.

$$V_{\text{oc-model}}(soc) = a_1 \cdot soc^7 + a_2 \cdot soc^6 + a_3 \cdot soc^5 + a_4 \cdot soc^4 + a_5 \cdot soc^3 + a_6 \cdot soc^2 + a_7 \cdot soc^1 + a_8 \tag{14}$$

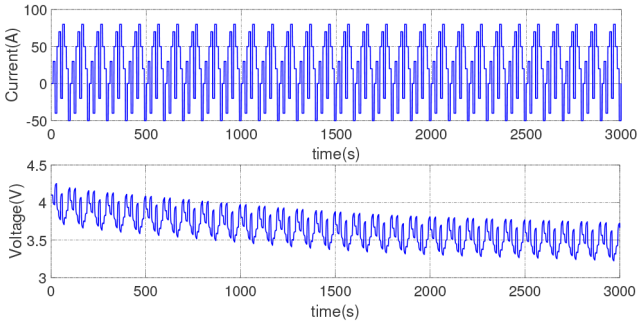

Fig. 5 *Current profile and battery output voltage*

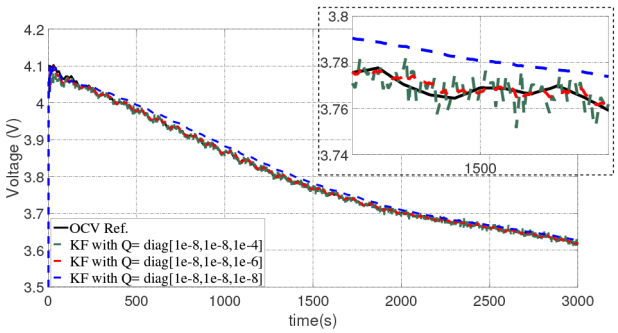

Fig. 6 *Impact of δ when estimating OCV with KF*

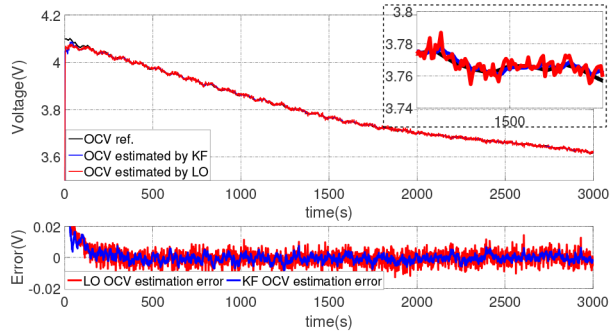

Fig. 7 *OCV estimation result with LO and KF*

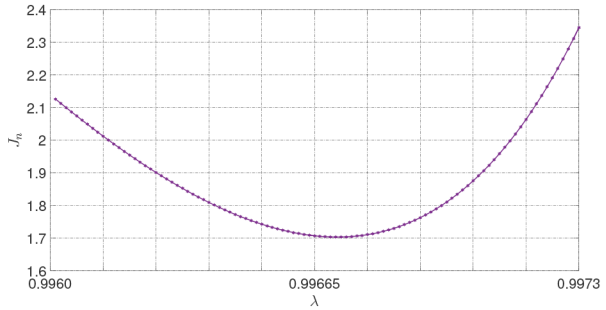

Fig. 8 *J_n versus λ*

Besides, the aging effect is not taken into account in our work with the following reasonable explanation, (i) lots of experiment-based LIB modelling works have verified this assumption, (ii) the usable range of SOC is usually controlled in a fixed interval in real application, 60–80% in our research work, for instance hence the OCV curve will be limited into a small segment, where the influence of the aging process can be ignored.

Besides, the well-known AH counting method is used as the model of SOC, which will be further considered as the reference value in our simulation studies [29]:

$$soc(t) = soc(t_0) - \eta \int_{t_0}^{t} \frac{I_{\text{batt}}(\tau)}{C_n} \mathrm{d}\tau \tag{15}$$

where η is the Columbic efficiency; C_n is the battery nominal capacity; $soc(t)$ is the required SOC in the time point t based on its initial value $soc(t_0)$.

Moreover, a dynamic current profile is designed in our work, as shown in Fig. 5, where the voltage response of the battery is also presented. The voltage data with the considered Gaussian white noise, whose statistical characteristic is set according to [30], will be fed to the four OCV estimation algorithms for this comparative study.

4.1 LO and KF

4.1.1 LO: For the discrete-time extended battery ECM (3), the pole placement strategy indicates that as long as all the eigenvalues of the matrix $(\boldsymbol{F} - \boldsymbol{KH})$ are located inside the unit circle of the complex plane, the above system is asymptotically stable [23]; in other words, the estimated states are able to converge to the real states of the system. Therefore, considering the convergence speed and the stability of the LO, a set of poles, $[0.43 + 0.2i,\ 0.43 - 0.2i,\ 0.9871]$, is elaborately selected after numerous simulation tests (i is the complex number $i^2 = -1$).

4.1.2 KF: The process noise and the measurement noise of the system (3) are set as follows: $\boldsymbol{Q} = \text{diag}[1 \times 10^{-8}, 1 \times 10^{-8}, \delta]$ and $R = 3.6 \times 10^{-5}$, where δ is the characteristic of the fictitious noise for the term V_{oc}; and it is of interest to note that δ will largely affect the OCV estimation result. Generally, the larger it is, the more dynamic the estimation will be, but the stability of the estimation will decrease at the same time.

For instance, three different values of δ, namely 1×10^{-4}, 1×10^{-6} and 1×10^{-8}, are selected in the simulation test. The KF is initialised with the vector $\boldsymbol{x}_0 = [0, 0, 3.5]$. The OCV estimation results are shown in Fig. 6. From these results, it is found that $\delta = 1 \times 10^{-6}$ is a good compromise between accuracy and stability. This value will be retained for the following comparison.

Here, the comparative study between the LO and KF for estimating the OCV is given firstly; both of them are initialised with the state vector $\boldsymbol{x}_0$, and the estimation result as well as the estimation error are shown in Fig. 7.

From Fig. 7, both LO and KF can track the OCV reasonably. However, as it can be seen from the estimation error, KF has better performance when estimating the OCV in the noisy environment.

4.2 FF-RLS and VFF-RLS

4.2.1 FF-RLS: In our simulation studies, inspired by the criterion (13), the forgetting factor λ of FF-RLS is selected by minimising the following criterion due to our interest in the OCV:

$$J_n = \sum_{k=1}^{L} [V_{\text{oc-model}}(k) - V_{\text{oc}}(k)]^2 \tag{16}$$

where $V_{\text{oc}}(k)$ is the inferred OCV from (8). L is equal to 3000, which is the length of the voltage vector. Besides, λ is usually close to 1, which can provide a rough search interval in our work. Hence, after several simulation tests, the desired forgetting factor $\lambda = 0.9967$ is selected for the FF-RLS according to Fig. 8.

4.2.2 VFF-RLS: Similarly, the criterion (16) will be used to select $\lambda_{\min}$ and ρ for the VFF-RLS. As shown in Fig. 9, the pair ($\lambda_{\min} = 0.7$, $\rho = 140$) is selected, while it is worth noting that the pair ($\lambda_{\min}$, ρ) can be selected in a relatively larger range compared with the determination of λ for the traditional FF-RLS. For instance, for the parameters in the red circled region in the 2D plot in Fig. 9, the VFF-RLS algorithm will roughly have the same performances. This can be regarded as robustness to the tuning.

The comparative study between FF-RLS and VFF-RLS for estimating the battery OCV is presented here. Both of these two algorithms are initialised by the parameter vector $\boldsymbol{\theta}_0 = [0.01; 0.01; 0.01; 0.01; 0.01; 0.01]$, and the result is shown in Fig. 10.

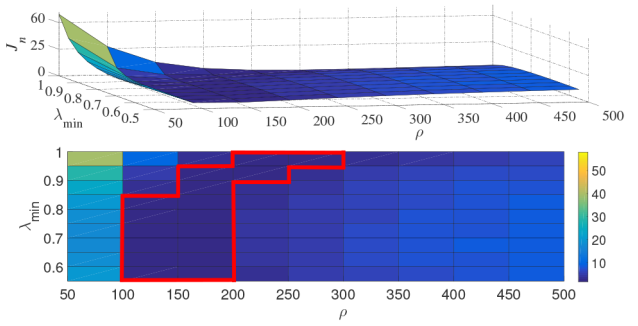

Fig. 9 *J_n versus λ_{min} and ρ in 3D and 2D*

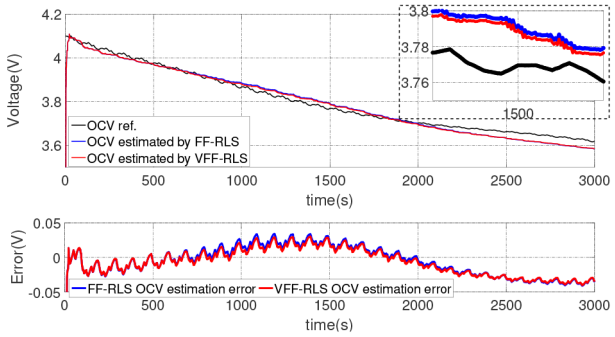

Fig. 10 *OCV estimation results with FF-RLS and VFF-RLS*

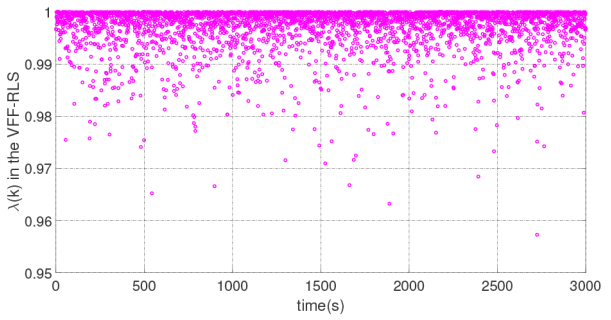

Fig. 11 *Variable forgetting factor during the operation*

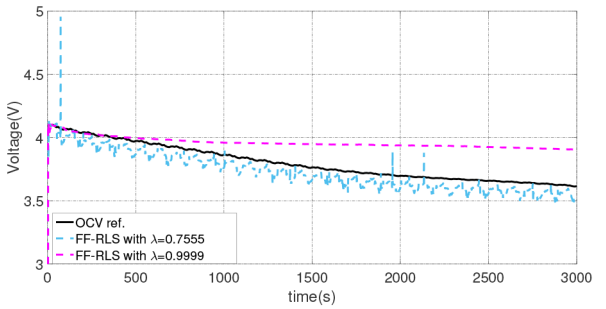

Fig. 12 *OCV estimation result with FF-RLS with $\lambda = 0.7555$ or $\lambda = 0.9999$*

Firstly, compared with observers, the regression-based OCV estimation has a very rapid convergence speed, because the initial value of OCV inferred by (8) with the initial parameter vector $\boldsymbol{\theta}_0$ is near zero, but they can still track the OCV within several recursive steps.

Secondly, according to the estimation error in Fig. 10, the VFF-RLS induces a limited improvement due to the variable forgetting factor, whose varying process is shown in Fig. 11. However, as discussed previously, VFF-RLS has parametric robustness. On the contrary, if the forgetting factor in FF-RLS is changed, for example $\lambda = 0.7555$ or $\lambda = 0.9999$, then the OCV estimation result shown in Fig. 12 will not meet the requirement for the SOC estimation.

5 Discussion

5.1 Accuracy and computational cost

As for the estimation accuracy and the computational cost, ten simulation tests are executed for the selected algorithms. The best-recorded estimation error mean value and the standard deviation of the estimation error for each method are presented in Table 1. The average calculation time of these ten simulation tests for each estimation method is also listed.

However, before concluding the estimation accuracy of different methods, a basic question needs to be considered: 'why we want to estimate the OCV?'. In fact, the answer, SOC estimation, is clearly presented in the introduction. Therefore, in this paper, the OCV estimation accuracy is evaluated in terms of the SOC estimation. Considering the studied SOC operation range in our work, namely 60–80%, the OCV model (14) is linearised as $V_{\text{oc - linearied}} = 0.7944 \times soc + 3.2899$, which will be used to infer the SOC by the estimated OCV in each iterative step as shown in Fig. 13.

Normally, SOC accuracy of 3–5% is required in the vehicle BMS [4]; hence, the ±3 and ±5% boundary of the model SOC, which can be regarded as the evaluation criterion, are presented directly in Fig. 13. Besides, the usable SOC range depends on the application. For example, the usable SOC range is larger in BEVs, because the battery is the main energy source. On the contrary, smaller SOC range is preferred in hybrid EVs, because this will protect the battery from premature aging. Considering a wider SOC range does not affect this comparative study. Because the methods of estimating the OCV value will always be the same, even in the wider SOC range. The difference lies in how to infer the SOC value from the OCV estimation. This is out of the scope of this comparative study. However, it can be achieved, for example by linearising the OCV-SOC curve over different SOC intervals.

KF has the best performance when estimating SOC; although the disadvantage of LO in coping with the noise will be reflected in the SOC estimation, both estimates are inside the ±3% accuracy boundary. The estimation of OCV by VFF-RLS remains in the ±5% accuracy boundary, while the FF-RLS has the worst performance in this comparison.

The result shown in Fig. 13 is consistent with the information in Table 1; KF has definitely the best performance in terms of the estimation accuracy, while LO is more attractive when considering the computational cost. Although regression-based estimation methods can converge rapidly, they have lower performance in terms of the estimation accuracy.

5.2 Robustness to model parameters

Since the parameters in the ECM will change due to many factors such as temperature and aging process, the discussion about the parametric robustness for the four algorithms will be more interesting than the robustness against the measurement noise, where KF is definitely the best.

In fact, for the OCV estimation, the parametric robustness of KF and LO is not as good as their estimation accuracy. Because the performances of KF and LO mainly rely on the model accuracy, however, the changing parameters in the ECM will undoubtedly result in the inaccuracy of the OCV estimation, and further, induce the invalid SOC estimation. For example, as shown in Fig. 14, the +30% ECM parameters change is introduced in the KF and LO, while the final inferred SOC is catastrophic.

On the contrary, all the parameters of the ECM will be updated for every iterative step in the FF-RLS and VFF-RLS. In other words, the OCV estimation by the FF-RLS and VFF-RLS can be considered as a result that already includes the parametric uncertainty of the battery ECM.

In addition, for KF and LO, although the ECM's parameters can be updated by further extending the system (3) using the same presented method. However, the high dimension of the corresponding matrixes of the extended model will become a heavy calculation burden for the BMS. Besides, the other two inevitable problems should be considered if the higher-dimensional extended model is used. Firstly, when extended with resistors and capacitors such as R_0, R_1, R_2, C_1 and C_2 the ECM model will become non-

Table 1 Comparison of the estimation methods

Criteria	FF-RLS	VFF-RLS	LO	KF
estimation error mean value, V	-2.60×10^{-3}	-1.70×10^{-3}	-1.88×10^{-4}	-1.78×10^{-4}
standard deviation of the estimation error, V	6.01×10^{-4}	4.93×10^{-4}	6.42×10^{-5}	2.25×10^{-5}
computational cost, s	0.046	0.049	0.011	0.056
robustness to model parameters	++	++	—	—
ease of tuning	+++	++	+	—

'+' means better performance.

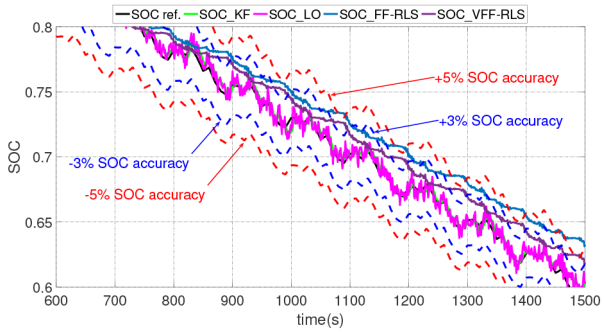

Fig. 13 *Comparison of the algorithms' accuracy*

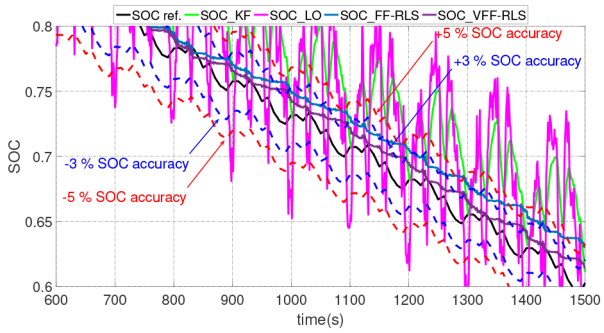

Fig. 14 *Response of SOC with +30% change of the ECM parameters in KF and LO*

linear. This will require the use of nonlinear filtering techniques, for example EKF and unscented KF. Therefore, this will increase the online calculation difficulty. Secondly, the observability of the non-linear extended model will be tedious to prove.

6 Conclusion

Parameter estimation, as an important approach for battery monitoring and fault diagnosis, is widely discussed around the battery resistance and battery capacity. However, studies about the battery OCV have great potential to further improve the battery's operation reliability. Hence, by reviewing the classical SOC estimation methods and several important characteristics of battery OCV, the importance and need for estimating the battery OCV have been introduced.

Then, based on the detailed modelling process of the extended battery model and ARX model, two OCV estimation methods are evaluated and compared. The first one uses observers for estimation based on state-space representation. The ARX model is developed to implement the regression-based OCV estimation methods.

From the evaluation of four estimation algorithms, the following conclusions can be drawn. KF has definitely better performances in a noisy environment. However, LO is very attractive for the vehicle BMS thanks to its lower computational cost. Although FF-RLS and VFF-RLS are robust to the model uncertainty and easy for tuning, it has been observed that their estimation results are poorer compared to observed-based methods.

The battery OCV estimation discussion presented in this paper is expected to bring a contribution to the battery OCV estimation and algorithm selection. Experimental validation could further support the simulation results and strengthen the conclusions drawn from the comparative study. Future research works should consider the following topics: (i) non-linear algorithms for battery parameters and state of health estimation; (ii) implementation issues of estimation algorithms on embedded battery management systems; (iii) energy management strategy optimisation including current battery state of health; (iv) development of efficient and reliable battery state of health and SOC prognosis.

7 References

[1] Waag, W., Fleischer, C., Sauer, D.U.: 'Critical review of the methods for monitoring of lithium-ion batteries in electric and hybrid vehicles', *J. Power Sources*, 2014, **258**, pp. 321–339

[2] Lu, L., Han, X., Li, J., *et al.*: 'A review on the key issues for lithium-ion battery management in electric vehicles', *J. Power Sources*, 2013, **226**, pp. 272–288

[3] Lai, X., Zheng, Y., Sun, T.: 'A comparative study of different equivalent circuit models for estimating state-of-charge of lithium-ion batteries', *Electrochim. Acta*, 2018, **259**, pp. 566–577

[4] Barillas, J.K., Li, J., Günther, C., *et al.*: 'A comparative study and validation of state estimation algorithms for li-ion batteries in battery management systems', *Appl. Energy*, 2015, **155**, pp. 455–462

[5] He, H., Xiong, R., Guo, H.: 'Online estimation of model parameters and state-of-charge of $LiFePO_4$ batteries in electric vehicles', *Appl. Energy*, 2012, **89**, (1), pp. 413–420

[6] Xia, B., Lao, Z., Zhang, R., *et al.*: 'Online parameter identification and state of charge estimation of lithium-ion batteries based on forgetting factor recursive least squares and nonlinear Kalman filter', *Energies*, 2018, **11**, (1), pp. 1–23

[7] Weng, C., Sun, J., Peng, H.: 'A unified open-circuit-voltage model of lithium-ion batteries for state-of-charge estimation and state-of-health monitoring', *J. Power Sources*, 2014, **258**, pp. 228–237

[8] Sidhu, A., Izadian, A., Anwar, S.: 'Adaptive nonlinear model-based fault diagnosis of li-ion batteries', *IEEE Trans. Ind. Electron.*, 2015, **62**, (2), pp. 1002–1011

[9] Pang, S., Farrell, J., Du, J., *et al.*: 'Battery state-of-charge estimation'. Proc. of the 2001 American Control Conf., Arlington, VA, USA, June 2001, pp. 1644–1649

[10] Pattipati, B., Balasingam, B., Avvari, G.V., *et al.*: 'Open circuit voltage characterization of lithium-ion batteries', *J. Power Sources*, 2014, **269**, pp. 317–333

[11] Zhang, C., Li, K., Pei, L., *et al.*: 'An integrated approach for real-time model-based state-of-charge estimation of lithium-ion batteries', *J. Power Sources*, 2015, **283**, pp. 24–36

[12] Rahimi-Eichi, H., Baronti, F., Chow, M.: 'Online adaptive parameter identification and state-of-charge coestimation for lithium-polymer battery cells', *IEEE Trans. Ind. Electron.*, 2014, **61**, (4), pp. 2053–2061

[13] Waag, W., Sauer, D.U.: 'Adaptive estimation of the electromotive force of the lithium-ion battery after current interruption for an accurate state-of-charge and capacity determination', *Appl. Energy*, 2013, **111**, pp. 416–427

[14] Gao, J., Shi, S., Li, H.: 'Brief overview of electrochemical potential in lithium ion batteries', *Chin. Phys. B*, 2016, **25**, (1), pp. 1–24

[15] Roscher, M.A., Sauer, D.U.: 'Dynamic electric behavior and open-circuit-voltage modeling of $LiFePO_4$-based lithium ion secondary batteries', *J. Power Sources*, 2011, **196**, (1), pp. 331–336

[16] Eichi, H.R., Chow, M.: 'Modeling and analysis of battery hysteresis effects'. IEEE Energy Conversion Congress and Exposition, Raleigh, NC, USA, September 2012, pp. 4479–4486

[17] Xiong, R., Yu, Q., Wang, L.Y., *et al.*: 'A novel method to obtain the open circuit voltage for the state of charge of lithium ion batteries in electric vehicles by using H infinity filter', *Appl. Energy*, 2017, **207**, pp. 346–353

[18] Tang, X., Mao, X., Lin, J., *et al.*: 'Li-ion battery parameter estimation for state of charge'. Proc. of the 2011 American Control Conf., San Francisco, CA, USA, July 2011, pp. 941–946

[19] Duong, V.H., Bastawrous, H.A., Lim, K., *et al.*: 'Online state of charge and model parameters estimation of the $LiFePO_4$ battery in electric vehicles using multiple adaptive forgetting factors recursive least-squares', *J. Power Sources*, 2015, **296**, pp. 215–224

[20] Zhang, C., Allafi, W., Dinh, Q., *et al.*: 'Online estimation of battery equivalent circuit model parameters and state of charge using decoupled least squares technique', *Energy*, 2018, **142**, pp. 678–688

[21] Chiang, Y.H., Sean, W.Y., Ke, J.C.: 'Online estimation of internal resistance and open-circuit voltage of lithium-ion batteries in electric vehicles', *J. Power Sources*, 2011, **196**, (8), pp. 3921–3932

[22] Åström, K.J., Wittenmark, B.: '*Adaptive control*' (Prentice-Hall, New Jersey, USA, 1994, 2nd edn.)

[23] Ogata, K.: '*Modern control engineering*' (Pearson, New Jersey, USA, 2009, 5th edn.)

[24] Plett, G.L.: 'Sigma-point Kalman filtering for battery management systems of LiPB-based HEV battery packs part 1: introduction and state estimation', *J. Power Sources*, 2006, **161**, (2), pp. 1356–1368

[25] Shi, Z.H.: 'Modeling and online aging monitoring of supercapacitors'. PhD thesis, Université de Nantes, 2014
[26] Paleologu, C., Benesty, J., Ciochina, S.: 'A robust variable forgetting factor recursive least-squares algorithm for system identification', *IEEE Signal Process. Lett.*, 2008, **15**, pp. 597–600
[27] Auger, F., Hilairet, M., Guerreo, J.M., *et al.*: 'Industrial applications of the Kalman filter: a review', *IEEE Trans. Ind. Electron.*, 2013, **60**, (12), pp. 5458–5471
[28] Lao, Z., Xia, B., Wang, W., *et al.*: 'A novel method for lithium-ion battery online parameter identification based on variable forgetting factor recursive least squares', *Energies*, 2018, **11**, (6), pp. 1–15
[29] Chen, Z., Fu, Y., Mi, C.C.: 'State of charge estimation of lithium-ion batteries in electric drive vehicles using extended Kalman filtering', *IEEE Trans. Veh. Technol.*, 2013, **62**, (3), pp. 1020–1030
[30] Zhao, S., Duncan, S.R., Howey, D.A.: 'Observability analysis and state estimation of lithium-ion batteries in the presence of sensor biases', *IEEE Trans. Control Syst. Technol.*, 2017, **25**, (1), pp. 326–333